Integrated Tunable Fiber Gratings for Dispersion Management in High-Bit Rate Systems

B. J. Eggleton, A. Ahuja, P. S. Westbrook, J. A. Rogers, P. Kuo, T. N. Nielsen, and B. Mikkelsen

***Abstract*—Dispersion management is becoming paramount in high-speed wavelength-division-multiplexed lightwave systems, that operate at per-channel rates of 40 Gb/s and higher. The dispersion tolerances, in these systems, are small enough that sources of dispersion variation, that are negligible in slower systems, become critically important to network performance. At these high-bit rates, active dispersion compensation modules may be required to respond dynamically to changes occurring in the network, such as variations in the per-channel power, reconfigurations of the channel's path that are caused by add-drop operations, and environmental changes, such as changes in ambient temperature. We present a comprehensive discussion of an emerging tunable dispersion compensating device, based on thermally actuated fiber gratings. These per-channel devices rely on a distributed on-fiber thin film heater, deposited onto the outer surface of a fiber Bragg grating. Current flowing through the thin film generates resistive heating at rates that are governed by the thickness profile of the metal film. A chirp in the grating is obtained by using a thin-film, whose thickness varies with position along the length of the grating in a prescribed manner; the chirp rate is adjusted by varying the applied current. The paper reviews some of the basic characteristics of these devices and their implementation, in a range of different applications, including the mitigation of power penalties associated with optical power variations. We present detailed analysis of the impact of group-delay ripple and polarization-mode dispersion on systems performance, and present results from systems experiments, that demonstrate the performance of these devices at bit rates of 10, 20, 40 and 160 Gb/s. We also discuss advantages and disadvantages of this technology, and compare to other devices.**

***Index Terms*—Dispersion compensation (DC), optical fiber communications, optical fiber dispersion, optical gratings, polarization mode dispersion (PMD), wavelength division multiplexing (WDM).**

I. Introduction

DYNAMIC dispersion compensation (DC) is becoming paramount in high-speed wavelength division multiplexing (WDM) lightwave systems, operating at 40 Gb/s and beyond. At these high bit rates, dispersion tolerances become small enough that variations in dispersion, which are negligible in slower systems, can severely influence network performance. In such systems, the amount of dispersion compensation, required at the receiver to maintain optimum systems performance, may vary in time because of several potential impairments. First, small variations in optical power, caused, for example, by imperfect gain flattening, can result in an additional nonlinear phase shift, that can modify the optimal dispersion map of the system [1], [2]. Second, dynamic reconfigurations of the network (e.g., channels originating from different locations) can change the total accumulated dispersion and nonlinear phase shift. Third, transmission conditions may change simply because of environmental variations, such as changes in ambient temperature [3]. For example, at communications wavelengths, the temperature dependence of the chromatic dispersion of a 2000-km span of nonzero-dispersion shifted fiber (NZDSF) is approximately 5 ps/nm/°C [3]. Therefore, given the allowable residual dispersion of ~50 ps/nm at 40 Gb/s, systems impairments are expected to occur with temperature changes as low as 10–20 °C. These problems are exacerbated by a reduced dispersion budget, associated with imperfect dispersion slope compensation over a wide bandwidth of operation, as well as small uncertainties in fiber dispersion. Consequently, systems operating at these high bit rates will require tunable dispersion compensators to dynamically adjust the dispersion map, preferably at the receiver and on a per-channel basis, to achieve compatibility with current network engineering rules.

The requirements on the bandwidth, group delay (GD) nonuniformity and polarization mode dispersion (PMD) of DC technologies become stringent at bit rates of 40 Gb/s and greater. Several tunable DC technologies devices have been demonstrated at lower bit rates. These include integrated all-pass filters, using ring-resonators [4] and so-called virtually imaged phased array devices [5]. Both devices have several desirable features, including a periodic response, which can allow for simultaneous dispersion compensation in multiple channels, and the possibility of dispersion slope compensation [4]. These devices are well suited to low bit rate multiple channel applications, however, because of an inherent tradeoff between dispersion and bandwidth, may not be well suited to high bit rate applications. Another option, which we discuss in detail in this paper, is tunable dispersion compensation, using chirped fiber Bragg gratings (CFBGs), which provides wavelength dependent GD when operated in reflection [6]. These devices can provide high dispersion, over bandwidths required for high bit rate applications, and provide significant tunability. They are, however, typically single channel devices, that require an optical circulator to retrieve the reflected signal, with the incurred expense and optical loss. Tunable dispersion is achieved typically by altering the chirp on the fiber grating with an externally applied perturbation.

Chirped fiber Bragg gratings have been demonstrated in two different contexts: First, CFBG have been demonstrated as

Manuscript received May 24, 2000; revised July 11, 2000.

B. J. Eggleton, A. Ahuja, P. S. Westbrook, J. A. Rogers, and P. Kuo are with Bell Laboratories, Lucent Technologies, Murray Hill, NJ 07974 USA (email: egg@lucent.com).

T. N. Nielsen and B. Mikkelsen are with Bell Laboratories, Lucent Technologies, Crawford Hill, Holmdel, NJ 07733 USA.

Publisher Item Identifier S 0733-8724(00)09103-9.

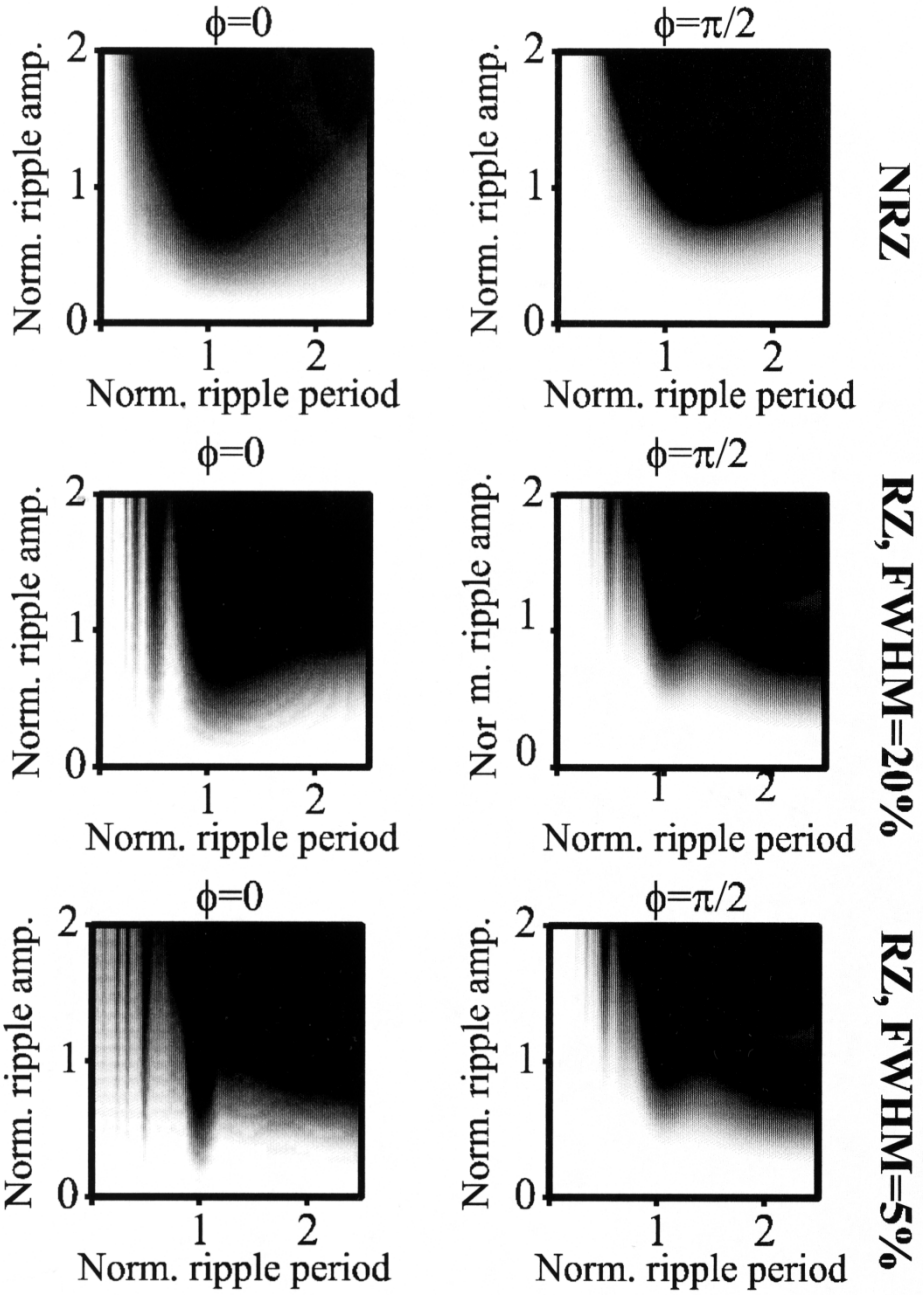

Fig. 1. Schematic illustration of possible embodiment for per-channel dispersion compensation device.

fixed DC devices with large dispersion, providing an alternative to conventional dispersion compensating fiber (DCF). Also, they have been used as per-channel devices, with relatively little dispersion for dispersion trimming, to be used in addition to DCF. In the former context, which we describe only briefly, CFBGs can provide several potential benefits, when compared to DCF, including reduced optical losses, reduced optical nonlinearity, and the possibility of complete dispersion slope compensation [7]–[10]. A number of impressive WDM systems experiments have been reported, using ultralong broad-band fiber gratings, demonstrating dispersion slope compensation and cascading multiple broad-band gratings [11]–[13]. In one experiment, Gnauck et al. [13] successfully transmitted 4×40 Gb/s optical time division multiplexing (OTDM) channels over 75 km, using a broad-band CFBG with dispersion of $D = -1300$ ps/nm. However, these experiments also revealed many of the deficiencies associated with such long broad-band CFBG. In particular, the GD nonuniformity and PMD [12] of ultralong CFBGs caused significant system penalty variations, as the signal wavelength is tuned across the CFBG reflection band. In addition, the bandwidth of such devices can be affected by short wavelength cladding mode loss exhibited by fiber Bragg gratings, as well as some loss induced by the holographic writing process.

This paper will focus on the application of *tunable* CFBGs as dispersion trimming elements. These devices use fiber Bragg gratings, with on-fiber integrated heaters to obtain tunable chirp and, thus, dispersion. The integrated heater consists of an ultra-

thin metal film, whose thickness varies along the length of the grating [14]–[19]. Flowing current through the film generates resistive heating at rates that vary with film thickness. The controllable temperature gradients along the length of the grating, generates chirp and, thus, dispersion, where the chirp can be adjusted reversibly by varying the applied current. Devices with *intrinsic* chirp inscribed in the holographic writing process, provide characteristics, that allow for implementation in systems operation at 40 Gb/s and above. These integrated devices satisfy many requirements for real-world applications, such as power efficiency, small size, simple fabrication and controllable optical properties. Such gratings are meant for operation on a per-channel basis to adjust dynamically dispersion and, thus, compensate for changes in network operating conditions [15]. In this context, the CFBG performs a complementary role to DCF, by providing a small amount of adjustable dispersion, allowing for real-time optimization of system performance [14]–[16]. As we demonstrate below, the GD nonuniformity and PMD properties of these relatively narrow-band per-channel tunable CFBG can meet the requirements of high-speed systems. The manufacturing tolerances of these devices are relaxed, compared to longer broad-band devices, and packaging becomes feasible. Incorporating devices into system receivers, as illustrated in Fig. 1, enables dispersion maps to be optimized, and power penalties, associated with previously mentioned impairments, to be reduced. Because the DC operation is performed on only a single channel after the signal is demultiplexed, the detrimental affects of cladding mode loss and out-of-band reflections are avoided, and cascading problems are not encountered, as the signal does not propagate significant distances after experiencing any limited device imperfections.

The paper is structured, as follows: in Section II, we describe the principle of operation of these devices, present a simple model for heat flow, that provides guidance for designing devices, and present device characteristics, including temporal response and power efficiency. In Section III, we describe briefly the fabrication of these devices. In Section IV, we describe the performance of these devices, including devices that incorporate intrinsic chirp to increase the usable bandwidth. In Section V, we discuss GD nonuniformities, and present simple analysis, that illustrates the impact of GD imperfections on systems performance. In Section VI, we present experimental results, that demonstrate the performance of tunable dispersion compensating CFBG in a variety of different systems experiments, with bit rates ranging from 10 to 160 Gb/s. We also show that such a device can be used to mitigate serious nonlinear signal distortion, associated with optical power variations. We conclude by highlighting some advantages and disadvantages of the devices in their current form, and several ways to improve their characteristics.

II. Device Design

Various authors have proposed schemes for obtaining tunable chirp in a fiber grating, either by uniform tuning of a nonlinearly CFBG [21], or by application of a nonuniform gradient, such as a temperature [22], or strain gradient [23]–[25] along the length of a uniform grating. The former scheme has been

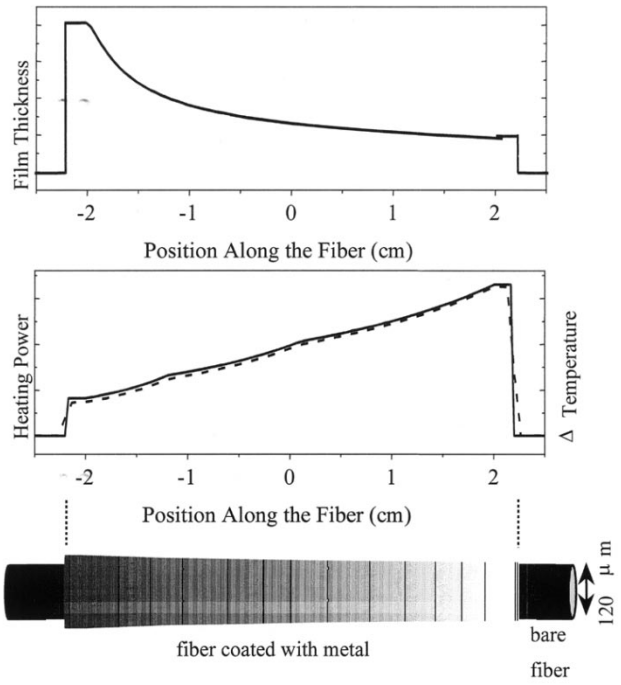

Fig. 2. Schematic of the device.

demonstrated in a range of applications at 10 Gb/s, including an implementation with a sampled grating, allowing for simultaneous dispersion compensation in several different channels [26]. The advantage of this scheme is that it can provide tunable DC, without requiring a nonuniform perturbation (e.g., temperature gradient). However, because of the inherent dispersion slope associated with the nonlinear chirp of these devices, they are limited to low bit rate applications. The latter scheme, which we consider in this paper, has the advantage that uniform dispersion can be provided, allowing for potential implementation in high-speed WDM lightwave systems ($\geq$40 Gb/s).

In thermally actuated devices, a gradient in temperature along the fiber causes a chirp in the grating, primarily because of the temperature dependence of the index of the glass [22]. Initial implementations of this type of device used a bulk heater, such as an oven and a refrigerator (or heat sink) connected to the ends of a thermally conductive plate with a v-groove, in which the fiber was mounted [22], [27]. The approximately linear temperature gradient, established in the material supporting the fiber, induced a similar gradient in the fiber. Although the performance of these devices could be acceptable for some applications, these bulk-heated devices were not well-suited to device applications, which require compactness, low power consumption, and mechanical stability. Moreover, this method does not allow for complex nonuniform chirps.

The integrated device that we consider, shown schematically in Fig. 2, relies on an integrated on-fiber thin-film heater deposited onto the outer surface of a fiber with an intra-core grating. The top frame shows a typical thickness distribution along the length of a grating; the middle frame shows the corresponding temperature distribution; and the bottom frame shows a schematic of the device. Current flowing though the thin film generates resistive heating, that has a spatial distribution determined by the thickness profile of the metal

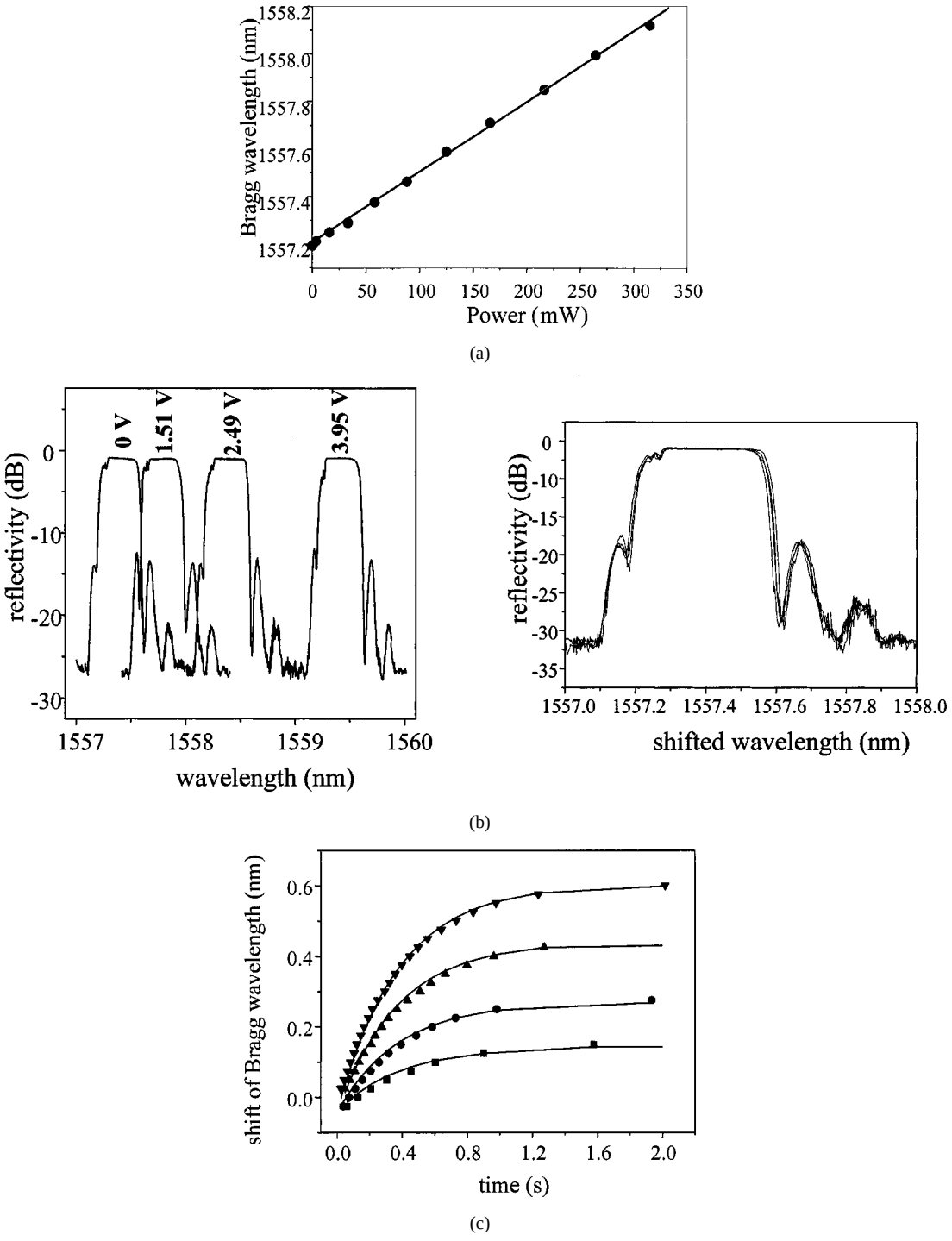

Fig. 3. (a) Plot of shift in Bragg wavelength of tunable grating with uniform thin-film heater. (b) Bragg grating reflection spectra at different heating levels and overlaid spectra show little distortion due to heating and (c) temporal response of device.

film [14], [18]. A uniform coating provides uniform heating power, and therefore, a uniform increase in temperature of the fiber [28]. Similarly, thermal gradients can be obtained by using a film, whose thickness varies with position along the length of the grating in a prescribed manner. The thickness profile of the film, in this case, determines the geometry of the temperature distribution, and the applied current defines the overall magnitude of the variation in the temperature.

The change in Bragg wavelength along the fiber, which defines the chirp, can be related to the film thickness, by making several assumptions about the fiber geometry and heat flow. Many of these assumptions are born out in experiments [15], [18], [29] and in full numerical simulations of the diffusion equation that are reported elsewhere [30]. The heating power, generated in the metal film along a short segment of fiber with length Δx and centered at a position x along the length of the fiber, is given by $P_{\rm in}(x)\Delta x = I^2 R(x)\Delta x$, where $P_{\rm in}(x)$ is the heating power per unit length at position x, I is the current (which, of course, is independent of position) and $R(x)$ is the local resistance per unit length of the metal. At steady-state,

the input power from the heating is equal to the rate of heat loss to the surroundings. Careful experiments demonstrate that, for typical operating temperatures, the loss of heat is directly proportional to the change in temperature [30]. It is possible, then, to write

$$P_{\text{in}}(x) - P_{\text{out}}(x) = I^2 R(x)\Delta x - a\Delta T(x)\Delta x = 0 \qquad (1)$$

where $\Delta T(x)$ is the change in temperature along the length of the fiber, and a is a constant, discussed further below, that relates this quantity to the rate of heat loss per unit length from the fiber. It follows from this equation that the change in the Bragg wavelength ($\Delta\lambda_B(x)$), which is related to the change in temperature by the thermo-optic coefficient, β, can be expressed as

$$\Delta\lambda_B(x) = \beta\Delta T(x) = \frac{\beta}{a} I^2 R(x). \qquad (2)$$

In order to induce a tunable linear chirp, the heating film must be designed, so that its resistance varies linearly with position. For films with thicknesses $t(x)$, small compared to the fiber diameter, $P_{\text{in}}(x,t) \propto I^2/t(x)$. It is then straightforward to show that, in this limit, a thin film whose thickness varies approximately inversely with position,

$$t(z) = \frac{A}{(z - B)} \qquad (3)$$

where z is the position along the fiber, A and B, constants that are determined by the thicknesses at the endpoints of the taper, produces an approximately linear temperature gradient [14]. There parameters are chosen to maximize the wavelength shift on the long wavelength side of the grating, and, at the same time, are selected to minimize the wavelength shift on the short wavelength side.

Devices that use integrated on-fiber heaters are attractive, in part because they have a remarkably low thermal mass, which allows them to be switched more quickly and operated with less power than conventional thermally actuated fiber devices (e.g., that described by Lauzon et al. [22]). Fig. 3(a) shows the measured Bragg wavelength shift as a function of applied electrical power, for a uniform grating with a uniform film, with a measured wavelength shift of ~2.0 nm/W. In this case (under uniform heating), one would expect the temperature change to cause only a shift and not any distortion of the spectrum. Fig. 3(b) shows reflection spectra from a Bragg grating under different heating levels, illustrating negligible distortion of the spectra (shown in the bottom frame). Fig. 3(c) shows the temporal response of this device, where the switching speed was determined for a range of different wavelength shifts (temperature changes). The temporal response was measured by applying a step function source of voltage to the integrated thin film and sequentially measuring, with a photodiode and a tunable laser, the arrival time of the edge of the reflection peak at various wavelengths. The solid lines is a theoretical fit, based on the heat-flow response [31]:

$$T(t) = \frac{P_{\text{IN}}}{a}(1 - e^{-at}) \qquad (4)$$

where we determine a $1/e$ time switching speed of 0.40 ± 0.05 s, corresponding to $a \sim 2.5\ \text{s}^{-1}$. Note that the rise and fall time (not shown here) are well-characterized by the single exponential, with a time constant that is independent of heating power.

III. Fabrication

Fabrication begins with the use of holographically generated phase masks and standard ultraviolet (UV) exposure techniques, to write suitably apodized chirped and unchirped gratings into the core of photosensitive fiber, stripped of its polymer jacket [32], [33]. With these procedures, we constructed unchirped and chirped gratings for tunable (~8 cm long) for adjustable DCs.

Several methods for fabricating tapered thin films have been developed, see [18] and [19] for more details. In the first method, removing the fiber from an electroplating bath with a programmable translation stage, while plating at constant current, produces a controlled variation in the thickness of the plated metal. Fig. 4(a) shows cross sectional micrographs of the ends of a typical coated fiber, fabricated using this method. The coating, which consists of a thin layer of silver (~10 μm) deposited onto titanium (~100 Å, as adhesion promoter) and gold (~1500 Å), was formed by electrodeposition, while the fiber was pulled at a controlled rate from a plating bath, in order to obtain the desired film thickness profile. Also shown in Fig. 4(a) (circles) are optical measurements of a fiber, in which the film thickness varies inversely with position along the length of the fiber; the film thickness varies from ~5 μm to ~50 μm, and the total resistance of the device is 0.8 Ω.

An alternative method, which is better suited than the electroplating technique for forming ultrathin films, uses electron beam evaporation and a moving shadow mask [19]. This approach to fabrication uses a computer-controlled, high precision rotation stage to move a shadow mask inside an electron beam evaporator. Coatings, with extremely well controlled variations in thickness, can be formed on many fibers in a single evaporation run. In this case, the film thickness can lie anywhere in the range from 0.2 to 2.0 μm, and is significantly less than the diameter of the fiber, as shown in Fig. 4(b), with a corresponding resistance from 50 to 100 Ω. This scheme has the added advantage that dual independently addressable films can be fabricated, allowing independent tuning of grating chirp and central wavelength [19]. This involves deposition of SiO_2 (~300 nm) onto the outer surface of the fiber, producing an electrically insulating coating on the gold, thus allowing for the deposition of a second layer. The layer of oxide insulates the gold films, so that they can be independently connected to and controlled by different power supplies. Also, the second film can be exploited to stabilize actively the tunable compensator against ambient temperature variations [34].

In both schemes, electrical connection to the films is provided by attaching fine wires to the ends of the metallized fiber with silver epoxy, providing electrical connection. Then, the grating is packaged (see Fig. 5) to provide thermal isolation, and thus ensure stable and reproducible operation of the device. Prior to packaging, the grating is annealed at high temperature to avoid any thermal degradation, associated with UV-induced defect relaxation [35].

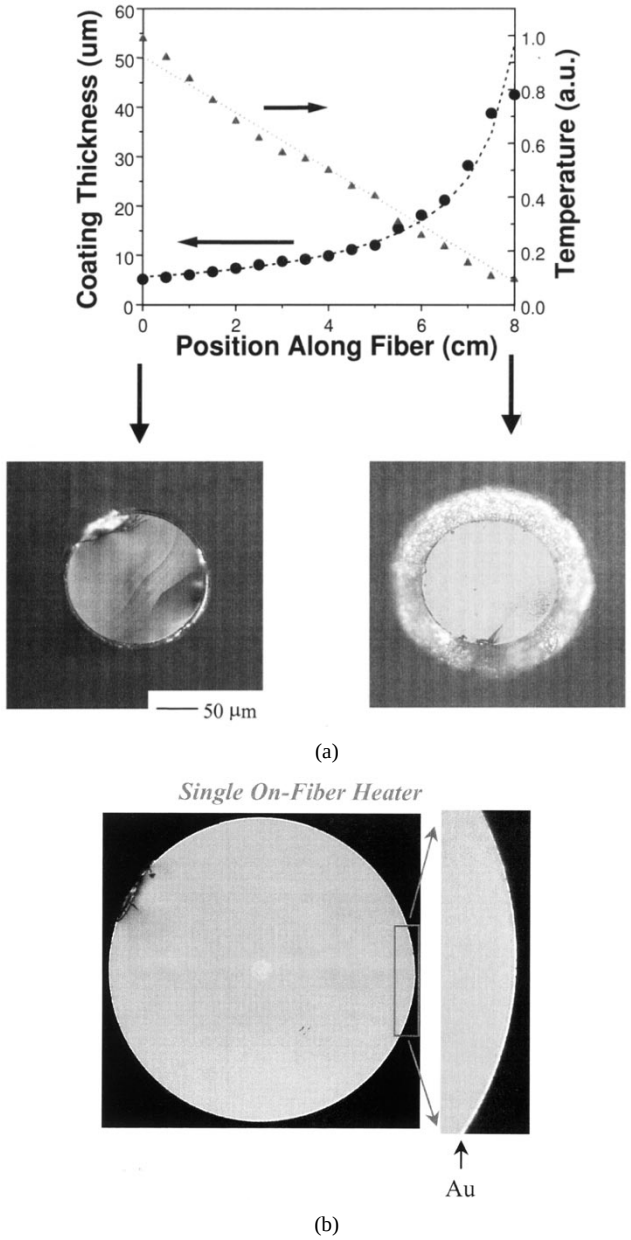

Fig. 4. (a) Circles: Thickness of a metal film plated onto the 7.5-cm fiber grating and theoretical fit based on profile designed to generate a linear temperature gradient. Triangles: Temperature distribution along the length of grating inferred from measured thickness profile and model described in text; line: linear fit. The lower frame shows cross-sectional optical micrographs of the plated fiber at the ends of the fiber grating. (b) Cross-sectional optical micrographs of fiber with a single thin-film of gold deposited onto the cladding region using electron-beam evaporation.

IV. Performance

In this section, we summarize optical characteristics of fiber gratings with tunable chirp, including designs that use gratings with intrinsic chirps. In Section V, we analyze GD ripple and PMD of these devices.

A. Fiber Grating with Tunable Chirp

A dispersion compensating device was fabricated, using the electron-beam evaporation technique described above, and was optimized to compensate about 800 ps/nm dispersion, enabling the fabrication of a very strong CFBG ($\kappa L \sim 20$) to maintain near-unity reflectivity over the device operation range, while minimizing GD variations arising from fiber and grating imperfections that have limited previous CFBGs. The grating was fabricated using an unchirped holographically generated phase mask with standard apodization. The tapered film was fabricated with a thickness profile, that varied inversely with position along the length of the grating, according to the discussion in Section III, with a thickness ratio of 3:1 ($\sim$0.6 μm to 0.2 μm).

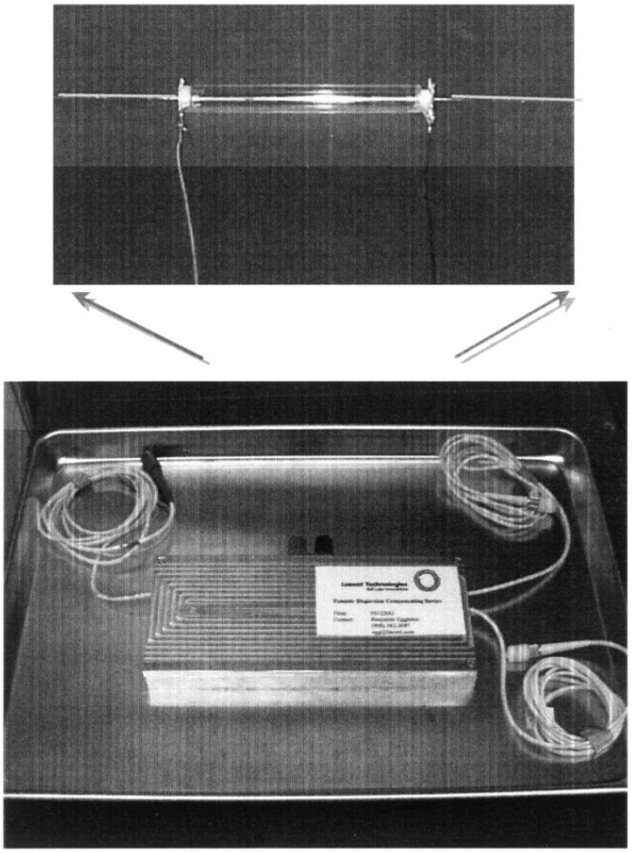

Fig. 5. Photo of simple package for integrated DC device.

Fig. 6(a) shows the broadening of the reflection spectrum, due to current-induced chirp in this device. The reflectivity of the grating is maintained above 98% for all values of applied voltage. Fig. 6(b) demonstrates the ability to control wavelength-dependent GD (dispersion) for the operating regime of the experiment described below. It also shows the measured group velocity dispersion as a function of applied voltage and a theoretical fit (dashed line) to the data using (3). GD was measured using the well-known modulation based commercial dispersion test set with modulation frequency of 2 GHz. Fig. 7 shows the deviations of the measured GD from linearity, with a peak-to-peak fluctuation of less than 10 ps. These data confirm the ability to engineer well-defined chirps by controlling the thickness profile of the thin-film heaters. Note, however, the shift in the short wavelength side of the reflection band, which is due to the finite thickness of the thin film at the cool end of the grating. Clearly, this limits the tunability of these devices; in this example, the tunability was limited to approximately 50 ps/nm. In the next section, we demonstrate devices optimized for 40 Gb/s with tunability of $>$200 ps/nm. As described below,

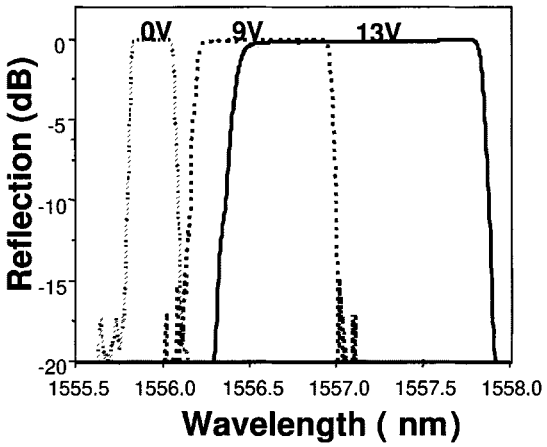

(a)

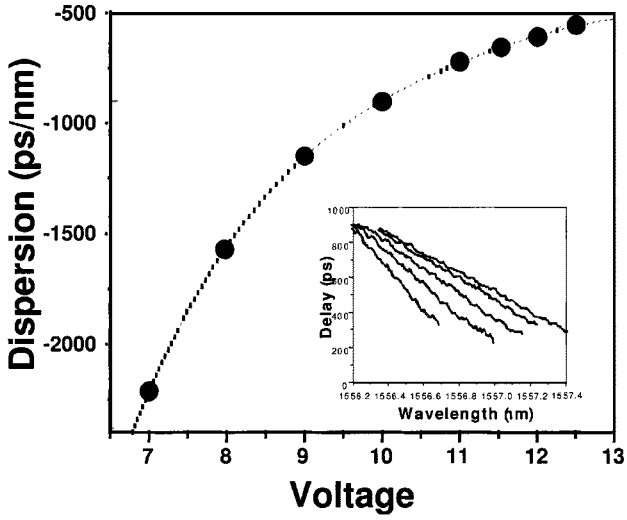

(b)

Fig. 6. (a) Reflection spectra for increasing applied current and (b) corresponding measured dispersion.

this increased bandwidth is achieved by increasing the ratio of the film thickness at the ends of the grating and using a grating with intrinsic chirp.

B. Tunable Fiber Grating with Intrinsic Chirp

By using an intrinsically chirped grating these devices can provide almost as much bandwidth with no input power as a device using a maximally tuned unchirped grating. This additional bandwidth is essential in high bit rate systems. For example, at 40 Gb/s, a single channel is nearly 0.8 nm wide; a per channel device must, therefore, provide at least 0.8 nm of bandwidth. Therefore, in order simply to accommodate a 40-Gb/s channel with a device that uses an initially unchirped grating (which typically has a bandwidth of 0.2 nm in the off state), the device must be heated by 60–80 °C. This result also implies that the device requires a constant supply of power in its entire operating range (for example, a typical unchirped device would require, a constant minimum supply of 0.2 W). Tunability then requires further increase in temperature (e.g., ∼200 °C). Moreover, devices optimized for implementation at 160 Gb/s, described in Section VI, require greater than 2 nm of optical bandwidth, which

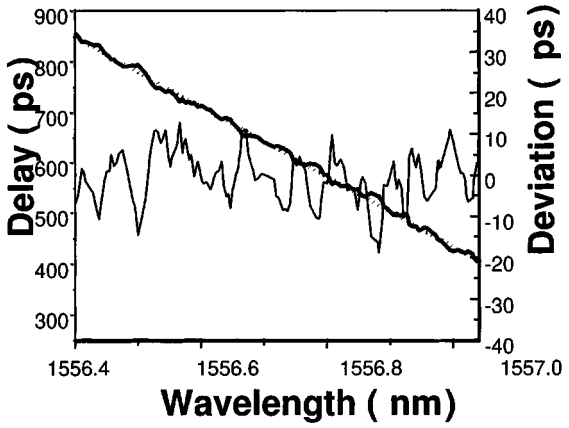

Fig. 7. Detailed dispersion characteristics and deviations from linearity.

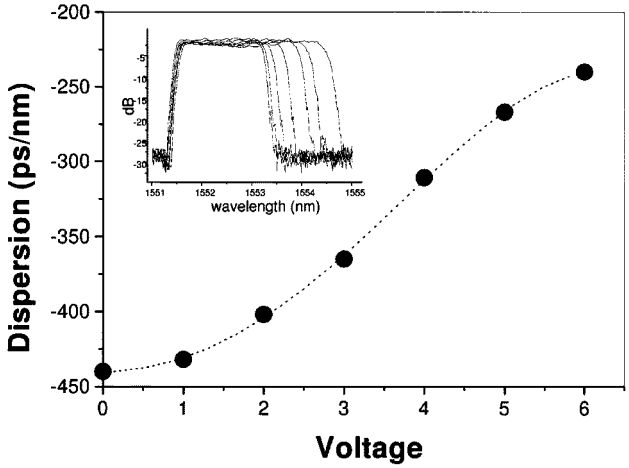

(a)

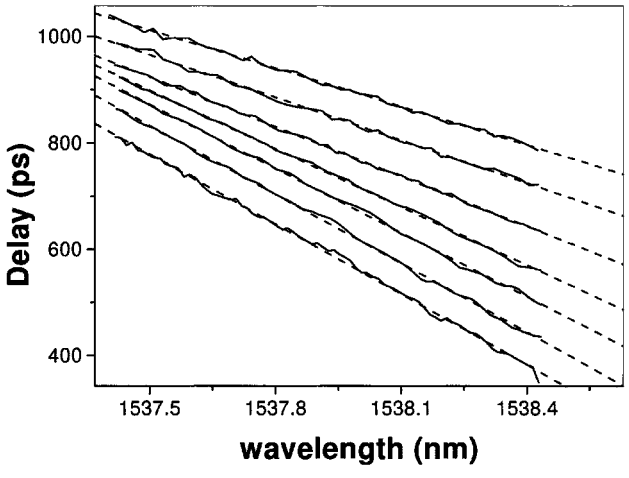

(b)

Fig. 8. (a) Measured dispersion as a function of applied voltage; inset shows reflection spectra. (b) GD characteristics of grating with intrinsic chirp.

would require ∼200 °C, and would not allow for significant tunability.

Fig. 8(a) and (b) show both the tunability and the dependence of dispersion on applied voltage for a typical device optimized for 40 Gb/s (intrinsic chirp of 0.175 nm/cm). Continuous dispersion tunability of up to 220 ps/nm is achieved, using intrinsically chirped devices and using a film profile with a ratio of 10:1

(thick end to thin end). The desired dispersion is obtained simply by increasing the applied voltage to the device from the power source. The input power required to tune maximally the devices is based on the resistance $(82.0 \pm 3.0\ \Omega)$ of the device and is <0.35 W. The intrinsic chirp in the grating means that a temperature gradient is not required to provide adequate bandwidth. More importantly for practical implementation, tunabilities of greater than 200 ps/nm can be obtained with absolute temperatures well below 200 °C (corresponding temperature gradients ∼25 to ∼175 °C above room temperature).

V. Systems Performance

A. Impact of Dispersion Ripple

An ideal dispersion compensation device would possess constant amplitude response, a GD that varies linearly with wavelength and exhibits no polarization dependence (i.e., polarization dependent loss or PMD). In practice, CFBG possesses both variations in amplitude and deviations in the GD. These imperfections are critical in determining the ultimate systems performance of these devices. They can manifest in eye closure and intersymbol interference (ISI), and result in variations in BER across the grating spectrum, a problem, which is of particular concern in long broad-band CFBGs [36]–[40]. These imperfections also manifest in tunable devices, such as those described in this paper, and can result in performance variations as the device is tuned. Although these imperfections are not fundamental to the grating, they are in practice very difficult to avoid. The GD variations can be microscopic [41] (i.e., rapid variations with wavelength) and can be attributed to random [42] or deterministic errors in the periodicity of the mask [43] used for the grating fabrication, variation in the fiber effective index [44] or associated with the UV exposure. Macroscopic variations, having longer periodicity, are seen often and can be attributed to nonperfect apodization of the grating [45], or the grating having nonideal chirp, for example due to a quadratic chirp in the phase mask [43]. In the context of the devices, we consider in this paper, macroscopic variations can also be caused by nonlinearities in the temperature distribution along the length of the fiber, due for example, to variations in film thickness [14].

Various authors have examined the impact of GD imperfections on systems performance, see [36]. We have analyzed numerically the power penalties associated with the imperfections in the GD response of CFBG for a range of different bit rates and data formats [37]. In this analysis, the GD imperfections are modeled as sinusoidal modulations of the GD response:

$$\mathrm{GD} = \frac{1}{2} A_{\mathrm{pp}} \times \cos\left[2\pi \frac{\Delta\lambda}{\lambda_p} + \varphi\right] \tag{5}$$

where A_{pp} is the peak-peak amplitude of the GD ripple in picoseconds normalized to the bit period. λ_p is the ripple period in picometers normalized to the single-sided spectral width of the signal, $\Delta\lambda$ (i.e., $\Delta\lambda = 80$ and $\Delta\lambda = 320$ pm for 10 and 40 Gb/s nonreturn-to-zero (NRZ), respectively). The ripple amplitude and periodicity are normalized, as their dependence on receiver penalty scales proportionally with the bit rate. ϕ is a phase constant, which determines whether the center wavelength of the modulated optical signal is aligned with the peak of the GD ripple (corresponding to $\phi = 0$) or the quadrature point of the GD ripple (corresponding to $\phi = \pi/2$).

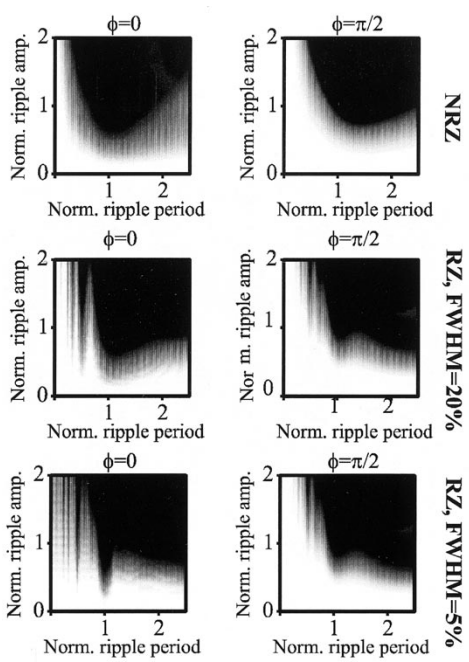

Fig. 9. Calculated power penalty versus normalized GD ripple periodicity and amplitude. Penalties range from 0 dB (white) to 2 dB and higher (black).

The penalties, calculated for the two cases, can differ substantially, depending on the period of the ripple. For example, for long ripple periods, the signal experiences predominately second-order dispersion, when the signal is aligned with the peak of a ripple, and predominately linear dispersion, when it is aligned with the quadrature point of a ripple. This gives rise to vastly different waveforms at the receiver, as e.g., second-order dispersion will tend to broaden the pulses asymmetrically, while linear dispersion leads to symmetrically broadened pulses [46]. While the effect of amplitude ripples on systems performance is well known [36], [37], we concentrate on GD ripples in this paper.

Fig. 9 shows the calculated penalties associated with a periodic GD variation for a NRZ and return-to-zero (RZ) signal, with the signal being aligned with a GD peak (left column), as well as the quadrature point of a GD ripple (right column). The calculated power penalties are color-coded ranging from 0 dB (white) to 2 dB and higher (black). In all calculations, the receiver was modeled as a PIN receiver followed by a fourth-order bessel filter with a bandwidth equal to the bit rate. BERs are calculated, assuming a Gaussian noise distribution, and the sampling point in the received eye is optimized in phase, as well as in amplitude (threshold) for minimum BER. Penalties are calculated as sensitivities at BERs of 10^{-9}, relative to the back-to-back configuration without GD imperfections. The length of the pseudorandom bit-stream (PRBS) sequence used in the simulations was $2^7 - 1$, and all modulation formats were unchirped. The bandwidth of the NRZ signal was equal to the bit rate, while RZ pulses were modeled as Gaussian with a fullwidth at half-maximum (FWHM) of 20% or 5% of the bitrate.

The simulations show that the worst case GD ripple period (in nm) and amplitude (in ps) are related to the bit rate. Independent of modulation format, the largest sensitivity to GD ripples occurs when the ripple period equals the bit rate corresponding to $\lambda_p = 1$ (e.g., 80 pm, for 10 Gb/s, 320 pm for 40 Gb/s and 1280 pm for 160 Gb/s). Using the worst case ripple period, penalties become unacceptable as the peak-to-peak amplitude of the GD ripples increases beyond half the bit period, i.e., less than 50 ps and 12.5 ps at 10 Gb/s and 40 Gb/s, respectively, and so forth.

The conclusion of our analysis and other earlier work [36] is that fast GD variations can only have minor system impacts for any of the modulation formats. Thus, the devices described in this paper, with peak-to-peak amplitudes of <10 ps ripple and ripple periods less than 100 pm (see Figs. 7–8), can meet the requirements of systems operating at bit rates of 40 Gb/s and higher. The reduced penalties at low ripple periods correspond to the case where $1/\lambda_p \rightarrow \infty$. Here, the phase (obtained by integrating the GD) added to the signal by the GD variation is oscillating rapidly with a magnitude proportional to $A_{\rm pp} * \lambda_p$. The phase shift induced on the signal, although highly nonlinear, thus has a very small magnitude, which explains qualitatively the $1/\lambda_p$ shape of the calculated penalties. The insensitivity to GD variation, with normalized ripple periods less than 1, is even more pronounced for low duty-cycle RZ. As we show below, systems penalty variations for 40 Gb/s and higher can be maintained at levels of below 1 dB.

B. Impact of Polarization Mode Dispersion

PMD is also known to be detrimental in high-speed systems. Various authors have investigated the impact of PMD in CFBG, [47]. PMD, also referred to as differential group delay (DGD) in CFBG, is due to birefringence in the fiber, either intrinsic to the fiber or induced in the UV writing process [48] or a combination of both. In a CFBG, where the GD in a linear function of wavelength, with dispersion: $|D|$, it is straightforward to show that [47]

$$\text{DGD} \sim 2|D|\Delta n\Lambda \tag{5}$$

where Δn is the linear birefringence of the core mode and Λ is the grating period. Although PMD has been limiting in many grating experiments, the measured DGD of these narrow-band tunable DC gratings can be kept below 1 ps, by use of photosensitive fiber with low birefringence and low UV-induced birefringence. Additionally, the dispersion of these devices is relatively low, making them less susceptible to PMD.

VI. Systems Experiments

A. Systems Performance

Fig. 10 shows the effect of the GD ripple of approximately 10 ps (device shown in Fig. 7), on system performance, where simulated and experimental system penalties across the grating reflection band are shown to be <0.3 dB at 10 Gb/s and <1 dB at 20 Gb/s.

Fig. 11 shows an example for a different device that was optimized for 40 Gb/s implementation (see Section IV). In this experiment, the grating was utilized to optimize the dispersion of a single span, comprising $\sim$40 km of standard single mode fiber,

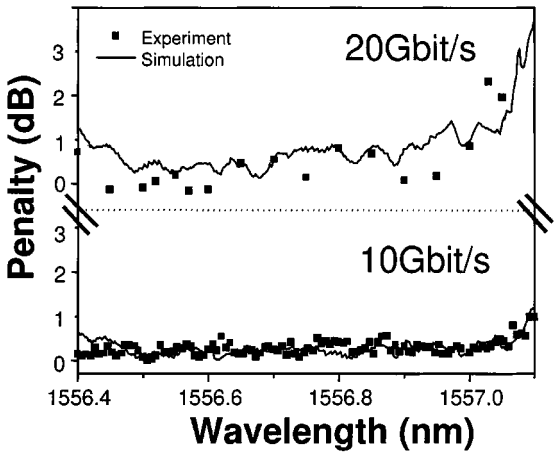

Fig. 10. The experimental (points) and simulated (line) system power penalty (at 10^{-9} BER) over the bandwidth of device for linear transmission.

operating at a bit rate of 40 Gb/s (NRZ). For each value of dispersion provide by the tunable grating the systems penalty was measured. The figure illustrates the performance of the device that exhibits less than 0.5 dB systems penalty when optimized. The eye diagrams illustrate the associated eye-closure. Below, we demonstrate the performance of these devices at bit rates of 40 and 160 Gb/s.

B. Mitigation of Nonlinear Penalties at 40 Gb/s

The dispersion tolerance of 40 Gb/s systems may be insufficient to accommodate the changes in dispersion, that can be expected to result from variations in the per-channel power levels, that can be anticipated due to imperfect gain flatness of optical amplifiers or reconfigurable add/drop [2], [49], [50]. The availability of tunable dispersion compensators could alleviate this problem by optimizing dynamically the dispersion map of the system to compensate for these changes in the per-channel power, as well as other variations. Although a linear device, such as a tunable CFBG, cannot restore completely a signal that is distorted by nonlinear effects, as we show below, it can reduce much of the incurred penalty, and enable an acceptable level of performance in a system thatotherwise would be nonfunctional. Here, we demonstrate that a tunable CFBG can be used as a per-channel postcompensator to reduce significantly the penalties that arise from variations in the per-channel launch power in a multi-span transmission system operating at 40 Gb/s NRZ, compared to a similar system with fixed dispersion compensation. We utilized the dispersion tunability of the grating to optimize dynamically the dispersion of a nonlinear system where the optimum degree of dispersion compensation changes with the power level.

The detailed GD deviation from linearity for this particular device (corresponding to a constant dispersion) is shown Fig. 12 for an applied voltage of 0.9 V, corresponding to a dispersion of -360 ps/nm. The figure also shows the simulated effect of this GD ripple of approximately 10 ps peak-to-peak as a 40 Gb/s NRZ signal is scanned across the bandwidth of the grating. The simulation includes an optically preamplified receiver model, and also accounts for the nonflat reflection of the grating. The low and uniform wavelength dependence of the calculated

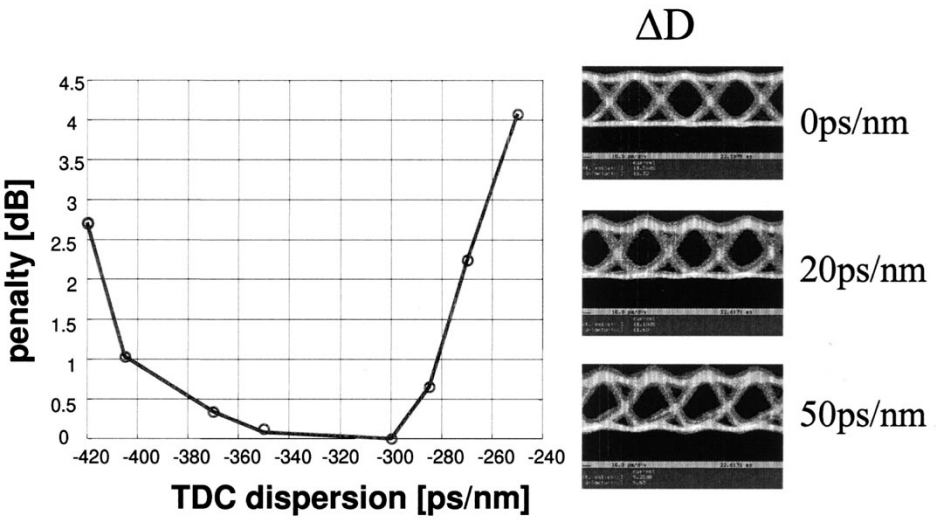

Fig. 11. Measured systems penalty (at 10^{-9} BER) for different values of adjustable dispersion. Inset shows corresponding eye-diagrams.

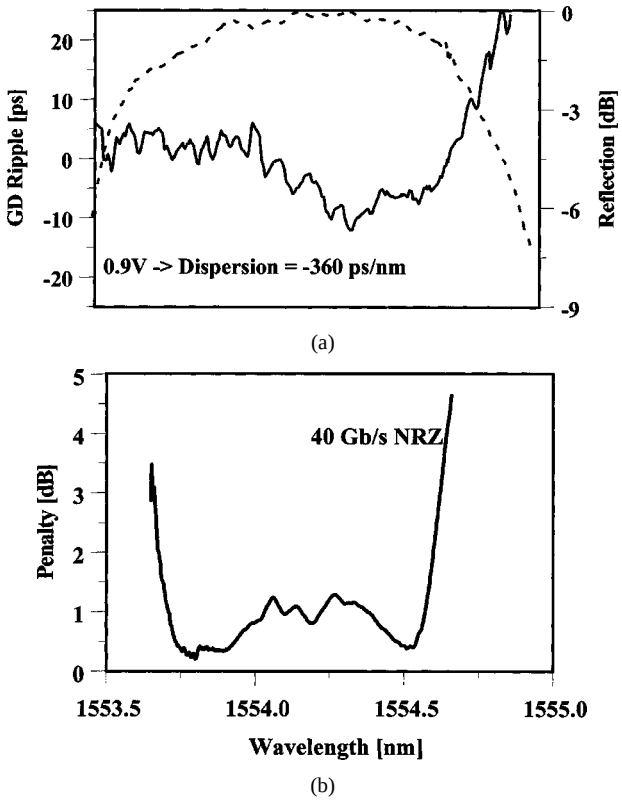

Fig. 12. (a) Measured reflection and ripple of FBG and (b) associated calculated penalty for optically preamplified 40 Gb/s NRZ signal.

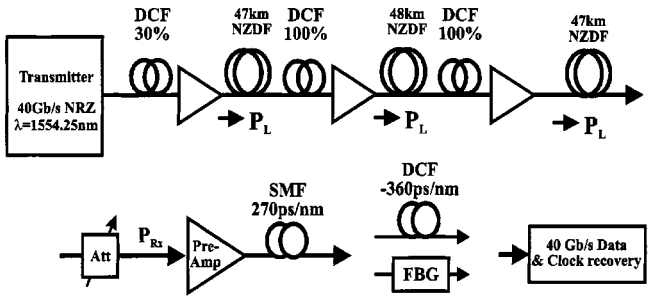

Fig. 13. Setup for the 40 Gb/s transmission experiment. Launch power, $\mathbf{P}_{\mathrm{L}}$, was varied from 0 to 13 dBm.

penalty is attributed to the low GD ripples, and the fact that the measured GD ripples generally have a periodicity smaller than the spectral width of the 40-Gb/s NRZ signal [36], [37].

We only assess the postcompensation implementation of the scheme, although the technique could be implemented in the pre-, post- or inline compensation modules of the system. The CFBG was placed at the receiver end of a 40-Gb/s NRZ transmission system consisting of three spans of NZDF, see Fig. 13. The length of the three fiber spans was chosen to be relatively short to avoid optical signal-to-noise ratio (SNR) limitations, as the launch power per span was varied from 0 to 13 dBm. Thus, we seek to measure and isolate the penalties caused by power dependent ISI penalties on the NRZ encoded PRBS of length $2^{31}-1$.

The dispersion map of the three-span transmission system was designed to enable a launch power of up to 9 dBm, before severe penalties were encountered, due to SPM. The dispersion of the NZDF was $+2.7$ ps/km/nm at 1555 nm, and DCF was used to provide 30% of precompensation and 100% inline compensation. The remaining 70% post compensation at the end of the three-span system was implemented in two ways. In one implementation, a fixed dispersion compensating module (DCF fiber with -360 ps/nm dispersion plus 15.9-km SMF with a dispersion of 17 ps/km/nm) was placed between the optical preamplifier and the 40 Gb/s receiver. The dispersion of the SMF and DCF modules was chosen to compensate fully the accumulated dispersion over the three spans of NZDF. Power into the DCF and SMF was kept low to avoid fiber nonlinearities. This dispersion map yields optimum dispersion compensation in the linear regime, i.e., at low launch power levels. Fig. 14 clearly illustrates the rapid increase in system penalties, due to fiber nonlinearities. Thus, with increasing launch power, the system becomes increasingly overcompensated, as SPM become significant. The figure also includes simulated results (solid line), and

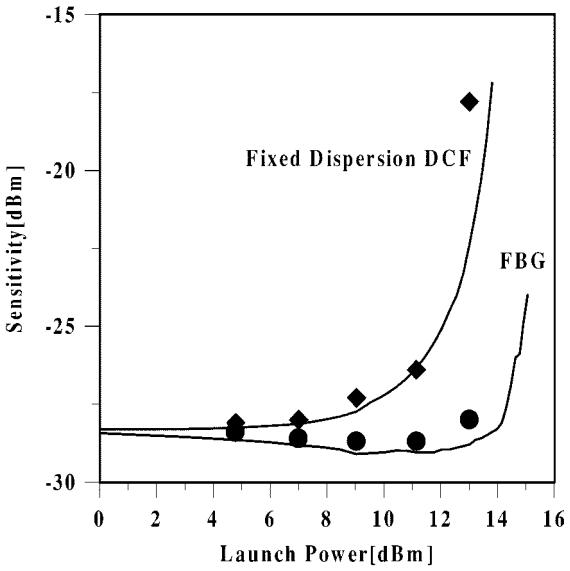

Fig. 14. Measured receiver sensitivity versus span launch power for system with fixed (diamonds) and optimized (circles) postdispersion compensation. Solid lines depicts simulated results.

as shown, we obtained good agreement between measured and simulated receiver sensitivities.

Next, the grating was used for the postdispersion compensator, instead of the DCF. By optimizing the dispersion of the grating at each power level, the power-dependent degradation in receiver sensitivity could be reduced greatly, compared to the configuration with a fixed amount post dispersion compensation. As seen, at 13 dBm of launch power, the ability to optimize the post dispersion can restore an otherwise completely deteriorated signal. The optimum dispersion of the FBG ranged from −360 ps/nm at 0 dBm launch power to −320 ps/nm at 13 dBm launch power. Indeed, the relatively small change in required dispersion highlights the fact that systems operating in the nonlinear regime become very sensitive to small changes in the dispersion.

Fig. 14 compares the measured receiver sensitivities to simulations, where the tunable dispersion compensator is assumed to have a perfect uniform dispersion equal to the optimum value for the specific power level. Thus, the deviation between the measured sensitivities obtained with the grating and the calculated results should reflect the penalty associated with the GD and reflection imperfections of the grating. As shown in Fig. 14, the deviation between the measured and simulated best case sensitivities was small, as expected from the results of Fig. 12. The close-to-ideal performance of the grating, despite its dispersion imperfections, can also be attributed to our specific application of the grating. Fig. 15 shows the recovered eye diagrams with fixed (left column) and tunable compensator (right column) in highly nonlinear lightwave system. Thus, by actively tuning the dispersion of the grating for optimum overall system performance, the impact of imperfections in the dispersion spectrum may be reduced greatly.

C. 160 Gb/s Systems Evaluations

Next generation time division multiplexed systems, operating at bit rates of 160 Gb/s, will require dispersion maps to be accurate to within ±7 ps/nm, corresponding to length accuracy's of ±400 m of standard single-mode fiber. At this bit rate, a tunable dispersion compensator will be essential to maintain systems performance. Moreover, electronic alternatives are not available at these bit rates, so the dispersion compensation must be all-optical. The tunable CFBG dispersion compensator was tested in the 160 Gb/s setup depicted in Fig. 15 [51].

By using a grating with a prescribed intrinsic chirp (chirp of 0.54 nm/cm), we provide sufficient bandwidth for operation at 160 Gb/s. Fig. 16(a) and (b) shows the measured reflectivity and dispersion of the device as a function of applied voltage. The

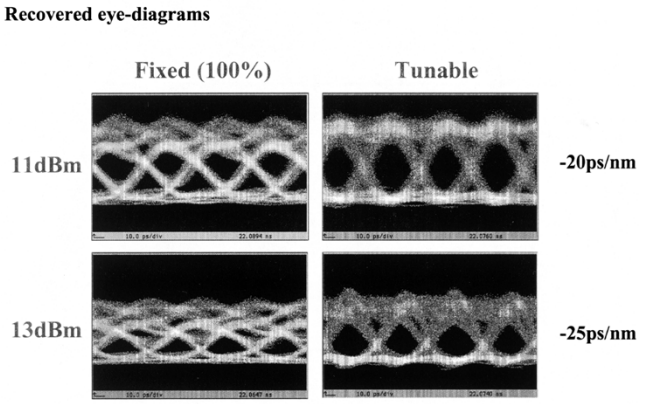

Fig. 15. Recovered eye diagrams with fixed (left column) and tunable compensator (right column) in highly nonlinear lightwave system.

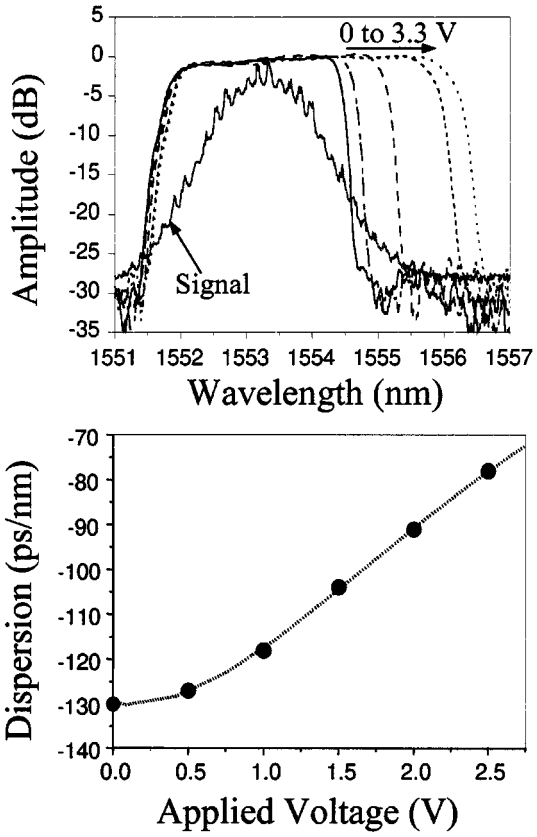

Fig. 16. (a) Measured reflectivity of tunable CFBG for different applied voltage. 160 Gb/s RZ signal spectrum is also shown. (b) Dispersion as function of applied voltage.

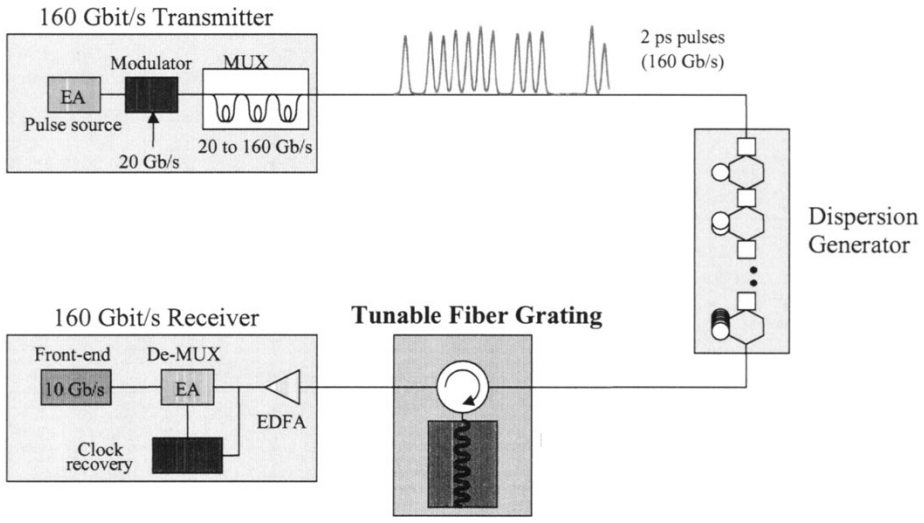

Fig. 17. Experimental set-up for test of tunable CFBG at 160 Gb/s.

tunable dispersion range of the device is -120 ps/nm to -60 ps/nm (0 to 3 V). The operating bandwidth of the device is >2.5 nm (sufficient for the 160 Gb/s RZ signal), and exhibits a GD nonuniformity <10 ps (peak-peak) with PMD of <0.1 ps. The fully packaged module, including optical circulator, exhibits an insertion loss of <2.5 dB. A critical performance improvement is realized since a majority of the GD nonuniformity occur at frequency less than the bit rate bandwidth, and the device is operated at the receiver.

A 160-Gb/s transmitter signal is realized by optical time division multiplexing of eight uncorrelated 20-Gb/s signals $(\mathrm{PRBS} = 2^{31} - 1)$ [52]. The duty cycle of the 160-Gb/s RZ signal is 30% (2 ps pulses), the FWHM optical bandwidth is 1.3 nm and the -10 dB bandwidth is 2 nm. The 160-Gb/s preamplified receiver employs two cascaded electroabsorption (EA) modulators to demultiplex optically from 160 to 10 Gb/s, where BER measurements are performed [52]. Clock-recovery is also performed by EA-modulators, as reported in [52].

The performance of the tunable CFBG dispersion compensator is investigated by inserting the CFBG after a dispersion generator, as shown in Fig. 18. The dispersion generator consists of a sequence of mechanical switches and different lengths of standard single-mode fiber and DCF. The module allows the dispersion to be preset between -200 and 200 ps/nm in steps of 1 ps/nm. Once the dispersion is preset, the CFBG compensates for the introduced dispersion, and BER performance is measured. As an example, Fig. 17 shows measured BER, when the tunable CFBG compensates for a dispersion of 90 ps/nm (voltage to CFBG is 2 V). The penalty is less than 1 dB, as compared with no dispersion.

The excellent performance of the CFBG is confirmed also by streak camera traces, as shown in Fig. 19, which shows recorded pulses, with and without the grating (net-dispersion is zero in both cases). The data rate is 80 Gb/s in this case, since the resolution of 3.5 ps of the streak camera prevent a 160-Gb/s data stream to be resolved clearly. The 80-Gb/s data rate is generated by blocking one of the arms in the last optical multiplexer in the transmitter; consequently, the pulses are still 2 ps wide, as for the 160-Gb/s data rate. As observed from the figure, the grating

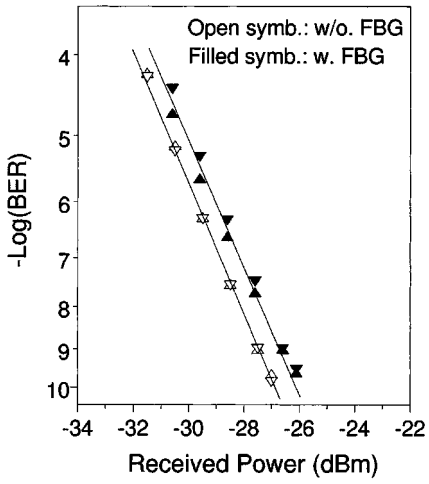

Fig. 18. Measured BER at 160 Gb/s with and without tunable CFBG. Net dispersion is zero in both cases.

only broadened the pulses marginally. Corresponding eye-diagrams as recorded with a 35-GHz photo-diode are also shown in the figure, showing clear eye-openings after the CFBG as well.

The tuning ability of the CFBG is illustrated in Fig. 20, which shows recorded receiver sensitivity at the data rate of 160 Gb/s for different amount of preset dispersion, being compensated by the CFBG. For comparison, the upper x-axis of the figure gives the measured sensitivity for different dispersion without the grating. Accepting a penalty of 2 dB for the preamplified receiver, the dispersion tolerance is ± 7 ps/nm without the CFBG, whereas the grating can compensate for a dispersion between 65 and 118 ps/nm, by varying the supplied voltage between 0.5 and 3.3 V. The figure also shows recorded eye-diagrams at 80 Gb/s (one arm of multiplexer blocked) for a dispersion of 20 ps/nm without the CFBG and a corresponding dispersion with the tunable grating. Clearly, for the case of a completely closed eye without the grating, the tunable dispersion compensator is able to provide an open eye. Similar performance is observed at 160 Gb/s, as illustrated by the eye-diagrams of the demultiplexed 10 Gb/s signals also shown in Fig. 20.

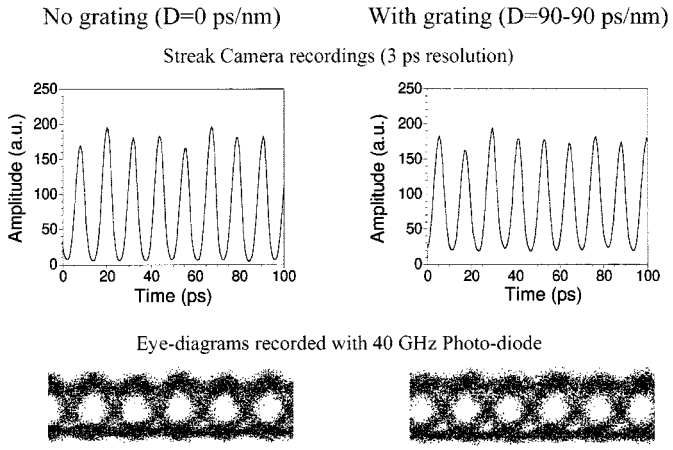

Fig. 19. Streak camera traces and eye-diagrams of 80-Gb/s signals, with and without tunable CFBG.

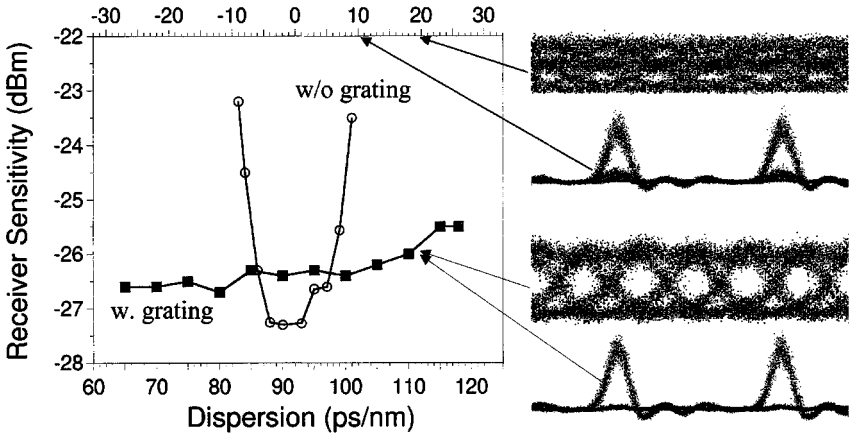

Fig. 20. Measured receiver sensitivity versus preset dispersion with (■) and without (O, upper axis) the tunable CFBG. Measured eye-diagrams at 80 and 160 Gb/s (after demultiplexing to 10 Gb/s) for different amount of preset dispersion.

VII. Conclusion

This paper has discussed the application of *tunable* CFBGs as dispersion trimming elements in high speed WDM lightwave systems. These devices use fiber Bragg gratings with on-fiber integrated heaters to obtain tunable chirp and thus dispersion. The integrated heater consists of an ultrathin-metal film whose thickness varies along the length of the grating. Flowing current through the film generates resistive heating at rates that varies with film thickness. The controllable temperature gradients along the length of the grating, generates chirp and thus dispersion, where the chirp can be adjusted reversibly by varying the applied current. These integrated devices satisfy many requirements for real-world applications, such as power efficiency, small size, simple fabrication and controllable optical properties. Such gratings are meant for operation on a per-channel basis to adjust dynamically dispersion, and thus compensate for changes in network operating conditions. We presented detailed analysis of the impact of group delay ripple and polarization mode dispersion on systems performance and presented results from systems experiments that demonstrate the performance of these devices at bit rates of 10, 20, 40, and 160 Gb/s. Although these devices can meet the demanding requirements of high-speed systems, they do have several disadvantages, most notably that they are per-channel devices and require an optical circulator to retrieve the reflected signal. Further improvements must be considered, including devices that can compensate multiple channels simultaneously, devices that provide PMD mitigation and for extremely high bit rates, such as 160 Gb/s, devices that provide intrachannel dispersion slope compensation.

Acknowledgment

The authors would like to thank M. Berger for providing the data used in Fig. 11.

References

[1] T. N. Nielsen, B. J. Eggleton, J. A. Rogers, P. B. Westbrook, P. B. Hansen, and T. A. Strasser, "Fiber Bragg grating tunable dispersion compensator for dynamic post dispersion optimization at 40 Gbit/s," *IEEE Photon. Technol. Lett.*, vol. 12, pp. 173–175, 2000.

[2] M. I. Hayee and A. E. Willner, "Pre- and post-compensation of dispersion nonlinearities in 10 Gb/s WDM systems," *IEEE Photon. Technol. Lett.*, vol. 9, pp. 1271–1273, 1997.

[3] W. H. Hatton and M. Nishimura, "Temperature dependence of chromatic dispersion in single mode fibers," *J. Lightwave Technol.*, vol. LT-4, pp. 1552–1555, 1986.

[4] C. K. Madsen, G. Lenz, A. J. Bruce, M. A. Cappuzzo, L. T. Gomez, and R. E. Scott, "Integrated all-pass filters for tunable dispersion and dispersion slope compensation," *IEEE Photon. Technol. Lett.*, vol. 11, pp. 1623–1625, 1999.

[5] L. D. Garrett, A. H. Gnauck, M. H. Eiselt, R. W. Tach, C. Yang, C. Mao, and S. Cao, "Demonstration of virtually-imaged phased-array device for tunable dispersion compensation in $16 * 10$ Gb/s WDM transmission over 480 km standard fiber," presented at the Optical Fiber Communications, Baltimore, MD, 2000, Postdeadline PD-7.

[6] F. Ouellette, "Dispersion cancellation using linearly chirped Bragg filters in optical waveguides," *Opt. Lett.*, vol. 12, pp. 847–849, 1987.

[7] R. Kashyap, H. G. Froehlich, A. Swanton, and D. J. Armes, "1.3 m long super-step-chirped fiber Bragg grating with a continuous delay of 13.5 ns and bandwidth 10 nm for broadband dispersion compensation," *Electron. Lett.*, vol. 32, pp. 1807–1809, 1996.

[8] R. Kashyap, *Fiber Bragg Gratings*, 1st ed. New York: Academic, 1999.

[9] L. Dong, M. J. Cole, A. D. Ellis, M. Durkin, M. Ibsen, V. Gusmeroli, and R. I. Laming, "40 Gbit/s 1.55 um transmission over 109 km of nondispersion shifted fiber with long continuously chirped fiber gratings," presented at the Optical Fiber Communications Conference, Dallas, TX, 1997.

[10] M. Ibsen, M. K. Durkin, K. Ennser, M. J. Cole, and R. I. Laming, "Long contiuosuly chirped fiber Bragg gratings for compensation of linear and 3rd order dispersion," in *Proc. ECOC'97*, vol. 2, 1997, pp. 49–52.

[11] L. D. Garrett, A. H. Gnauck, F. Forghieri, V. Gusmeroli, and D. Scarano, "16×10 Gb/s WDM transmission over 840 km SMF using eleven broadband chirped fiber gratings," presented at the ECOC'97, 1997, Paper TuC05.

[12] A. H. Gnauk, L. D. Garrett, F. Forghieri, V. Gusmeroli, and D. Scarano, "$8 * 20$ Gb/s-315 km, $8 * 10$ Gb/s-480 km WDM transmission over conventional fiber using multiple broad-band fiber gratings," *IEEE Photon. Technol. Lett.*, vol. 10, pp. 1495–1497, 1998.

[13] A. H. Gnauk, J. M. Weisenfield, L. D. Garrett, R. M. Derosier, F. Forghieri, V. Gusmeroli, and D. Scarano, "$4 * 40$ Gb/s 75 km WDM transmission over conventional fiber using a broad-band fiber grating," *IEEE Photon. Technol. Lett.*, vol. 11, pp. 1503–1505, 1999.

[14] B. J. Eggleton, J. A. Rogers, P. B. Westbrook, and T. A. Strasser, "Electrically tunable power efficient dispersion compensating fiber Bragg grating," *IEEE Photon. Technol. Lett.*, vol. 11, pp. 854–856, 1999.

[15] B. J. Eggleton, J. A. Rogers, P. B. Westbrook, T. A. Strasser, T. N. Nielsen, P. B. Hansen, and K. F. Dreyer, "Electrically tunable power efficient dispersion compensating fiber Bragg grating for dynamic operation in nonlinear lightwave systems," presented at the Optical Fiber Communications Conference, San Diego, CA, 1999, Postdealine Paper PD-27.

[16] B. J. Eggleton, T. N. Nielsen, J. A. Rogers, P. S. Westbrook, P. B. Hansen, and K. F. Dreyer, "Dispersion compensation in 20 Gbit/s dynamic nonlinear lightwave systems using electrically tunable chirped fiber grating," *Electron. Lett.*, vol. 35, pp. 832–834, 1999.

[17] B. J. Eggleton, J. A. Rogers, P. S. Westbrook, G. Burdge, S. Ramachandran, A. A. Abramov, T. N. Nielsen, G. R. Kowach, R. S. Windeler, and T. A. Strasser, "Tunable fiber grating devices utilizing integrated thin film heaters," in *WDM Components*, D. A. Nolan, Ed. Washington, DC: Optical Society of America, 1999, vol. XXIX, pp. 61–72.

[18] J. A. Rogers, B. J. Eggleton, J. R. Pedrazzani, and T. A. Strasser, "Distributed on-fiber thin film heaters for fiber Bragg gratings with adjustable chirp," *Appl. Phys. Lett.*, vol. 74, pp. 3131–3133, 1999.

[19] J. A. Rogers, B. J. Eggleton, R. J. Jackman, G. R. Kowach, and T. A. Strasser, "Dual on-fiber thin film heaters for fiber gratings with independently adjustable chirp and wavelength," *Opt. Lett.*, vol. 24, pp. 1328–1330, 1999.

[20] A. E. Willner, K.-M. Feng, J.-X. Cai, S. Lee, J. Peng, and H. Sun, "Tunable compensation of channel degrading effects using nonlinearly chirped passive fiber Bragg gratings," *IEEE J. Select. Topics Quantum Electron.*, vol. 5, pp. 1298–1311, 1999.

[21] K.-M. Feng, J.-X. Cai, V. Grubsky, D. S. Starodubov, M. I. Hayee, S. Lee, X. Jiang, A. E. Willner, and J. Feinberg, "Dynamic dispersion compensation in a 10 Gbit/s optical system using a voltage controlled tuned nonlinearly chirped fiber Bragg grating," *IEEE Photon. Technol. Lett.*, vol. 11, pp. 373–375, 1999.

[22] J. Lauzon, S. Thibault, M. J, and F. Ouellette, "Implementation and characterization of fiber Bragg gratings linearly chirped by temperature gradient," *Opt. Lett.*, vol. 19, pp. 2027–2029, 1994.

[23] P. C. Hill and B. J. Eggleton, "Strain gradient chirp of fiber Bragg grating," *Electronics Letters*, vol. 30, pp. 1172–1174, 1994.

[24] M. Pacheco, A. Medez, L. A. Zenteni, and F. Mendoz-Santoyo, "Chirping optical fiber Bragg gratings using tapered-thickness piezoelectric ceramic," *Electron. Lett.*, vol. 34, pp. 2348–2350, 1998.

[25] M. M. Ohn, A. T. Alavie, R. Maaskant, M. G. Xu, F. Bilodeau, and K. O. Hill, "Dispersion variable fiber grating using a piezoelectric stack," *Electron. Lett.*, vol. 32, pp. 2000–2001, 1996.

[26] J.-X. Cai, K.-M. Fend, A. E. Willner, V. Grubsky, D. S. Starodubov, and J. Feinberg, "Simultaneous tunable dispersion compensation of many WDM channel using a sampled nonlinearly chirped fiber Bragg grating," *IEEE Photon. Technol. Lett.*, vol. 11, pp. 1455–1457, 1999.

[27] S. Barcelos, M. N. Zervas, R. I. Laming, D. N. Payne, L. Reekie, J. A. Tucknott, R. Kashyap, P. F. Mkfee, F. Sladen, and B. Wojciechowicz, "High accuracy dispersion measurements of chirped fiber gratings," *Electron. Lett.*, vol. 31, pp. 1280–1281, 1995.

[28] H. G. Limberger, N. H. Ky, D. M. Costantini, R. P. Salathe, C. A. P. Muller, and G. R. Fox, "Efficient miniature fiber-optic tunable filter based on intracore Bragg grating and electrically resistive coating," *IEEE Photon. Technol. Lett.*, vol. 10, pp. 361–363, 1998.

[29] B. J. Eggleton, A. A. Abramov, J. A. Rogers, R. P. Espindola, A. Hale, R. S. Windeler, and T. A. Strasser, "Electrically tunable broadband long period fiber grating filter," presented at the CLEO, Baltimore, MD, 1999, Paper CMC3.

[30] J. A. Rogers, P. Kuo, A. Ahuja, B. J. Eggleton, and R. J. Jackman, "Analysis of heat flow in optical fiber devices that use integrated thin film heaters," *Appl. Opt.*, 2000.

[31] H. S. Carslaw and J. C. Jaeger, *Conduction of Heat in Solids*, 2nd ed. London, U.K.: Oxford University Press.

[32] J. Martin and F. Ouellette, "Novel writing techniques of long in-fiber gratings," *Electron. Lett.*, vol. 30, pp. 811–812, 1993.

[33] T. A. Strasser, P. J. Chandonnet, J. DeMarko, C. E. Soccolich, J. R. Pedrazzani, D. J. Digiovanni, M. J. Andrejco, and D. S. Shenk, "UV-induced fiber grating OADM devices for efficient bandwidth utilization," in *Proc. Optical Fiber Communications*, 1996, Postdeadline Paper PD8-1.

[34] J. A. Rogers, B. J. Eggleton, and P. Kuo, "Temperature stabilized operation of tunable fiber grating devices that use distributed on-fiber thin film heaters," *Electron. Lett.*, vol. 35, pp. 2052–2053, 1999.

[35] T. Erdogan, V. Mizrahi, P. J. Lemaire, and D. Monroe, "Decay of ultraviolet-induced fiber Bragg gratings," *J. Appl. Phys.*, vol. 76, pp. 73–80, 1994.

[36] K. Ennser, M. Ibsen, D. Durkin, M. N. Zervas, and R. I. Laming, "Influence of nonideal chirped grating characteristics on dispersion," *IEEE Photon. Technol. Lett.*, vol. 10, pp. 1476–1478, 1999.

[37] T. N. Nielsen, B. J. Eggleton, and T. A. Strasser, "Penalties associated with group delay imperfection in optical components for NRZ, RZ and duo-binary encoded signals," presented at the ECOC'99, Nice, France, 1999.

[38] V. Gusmeroli and D. Scarano, "Fiber grating dispersion compensators," presented at the Optical Fiber Communications, San Diego, CA, 1999, Paper FA4.

[39] S. G. Evangelides, N. S. Bergano, and C. R. Davidson, "Intersymbol interference induced by ripple in fiber Bragg gratings," presented at the Optical Fiber Communications, San Diego, CA, 1999, Paper FA2.

[40] H. Rourke, B. Pugh, S. Kanellopoulos, V. Baker, B. Napier, P. Greene, D. Goodchild, J. Fells, R. Epworth, and A. Collar, "Fabrication and systems performance of dispersion compensation gratings," in *Proc. European Conference on Optical Communications*, vol. 1, Nice, France, 1999, pp. 165–167. presented at.

[41] F. Ouellette, "The effect of noise on the spectral response of fiber gratings," in *Bragg Gratings, Photosensitivity, and Poling in Glass Fibers and Waveguides: Properties and Applications*, Williamsburgh, VA, 1997, Paper BMG13.

[42] R. Feced and M. N. Zervas, "Effects of random noise and amplitude errors in optical fiber Bragg gratings," *J. Lightwave Technol.*, vol. 18, pp. 90–100, 2000.

[43] S. J. Mihailov, F. Bilodeau, K. O. Hill, D. C. Johnson, J. Albert, D. Stryckman, and C. Shu, "Comparison of fiber Bragg grating dispersion-compensators made with holographic and E-beam written phase masks," *IEEE Photon. Technol. Lett.*, vol. 11, pp. 572–574, 1999.

[44] M. Ibsen and R. I. Laming, "Fiber nonuniformity caused Bragg grating imperfections," presented at the Optical Fiber Communications, San Diego, CA, 1999, Paper FA1.

[45] L. Poladian, "Analysis and modeling of group delay ripple in Bragg gratings," presented at the Bragg Grating, Photosensitivity, and Poling in Glass Waveguides, Stuart, FL, 1999, Paper SaA4.

[46] G. P. Agrawal, *Nonlinear Fiber Optics*. San Diego, CA: Academic Press, 1989.

[47] M. Schiano and G. Zaffiro, "Polarization mode dispersion in chirped fiber gratings," in *European Conf. Optical Communications*, vol. 1, Madrid, Spain, 1998, pp. 403–404.
[48] T. Erdogan, V. Mizrahi, P. J. Lemaire, and D. Monroe, "Decay of ultraviolet-induced fiber Bragg gratings," *J. Appl. Phys.*, vol. 76, pp. 73–80, 1994.
[49] F. Forghieri, "WDM systems impairments," presented at the Dig. Optical Fiber Communication Conf., San Diego, CA, 1999, Paper WF.
[50] Y. Frignac and S. Bigo, "Numerical optimization of residual dispersion in dispersion-managed systems at 40 Gbit/s," presented at the Optical Fiber Communication, Baltimore, MD, 2000, Paper TuD3-1.
[51] B. J. Eggleton, B. Mikkelsen, G. Raybon, A. Ahuja, J. A. Rogers, P. S. Westbrook, T. N. Nielsen, S. Stulz, and K. Dreyer, "Tunable dispersion compensation in a 160 Gb/s TDM system by a voltage controlled chirped fiber Bragg grating," *IEEE Photon. Technol. Lett.*, vol. 12, pp. 1022–1024, Aug. 2000.
[52] B. Mikkelsen, G. Raybon, R.-J. Essiambre, K. Dreyer, Y. Su, L. E. Nelson, J. E. Johnson, G. Shtengel, A. Bond, D. G. Moodie, and A. D. Ellis, "160 Gbit/s single-channel transmission over 300 km nonzero-dispersion fiber with semiconductor based transmitter and demultiplexer," in *Proc. ECOC'99*, Nice, France, 1999, Postdeadline Paper PD 2.3.

Benjamin J. Eggleton received the Bachelor degree with Honors in physics from the University of Sydney, Sydney, New South Wales, Australia. He received the Ph.D. degree from the School of Physics and the Optical Fiber Technology Center, the Australian Photonics Cooperative Research Center at the University of Sydney, in 1996. His doctoral research focused on linear and nonlinear effects in fiber gratings.

From November 1996 to June 1998, he was a Postdoctoral Member of Technical Staff in the Department of Optical Physics at Bell Laboratories, Lucent Technologies, Murray Hill, NJ. In July 1998, he joined the Optical Fiber Research Department at Bell Laboratories, as a Member of Technical Staff. His research interests include nonlinear optics, Bragg soliton phenomena, fiber optics, fiber gratings, photonic bandgap structures, air-silica microstructured optical fibers, all-optical switching devices, and dispersion compensation techniques in WDM lightwaves systems.

Dr. Eggleton was awarded the 1998 Adolph Lomb Medal from the Optical Society of America for his research which involved the first observation of nonlinear propagation effects in photonic bandgap structures.

A. Ahuja, photograph and biography not available at the time of publication.

Paul S. Westbrook receive the Ph.D. degree in physics from the Massachusetts Institute of Technology, Cambridge, in 1998, and joined the staff of Bell Laboratories in 1998 as a Postdoctoral Researcher in the fiber devices research area. He is currently a Member of Technical Staff at Bell Laboratories in the area of fiber waveguide research and has worked on several topics including in-fiber polarization monitoring and control, hybrid polymer-silica fibers, air-silica microstructure fibers, and dispersion compensating fiber gratings.

John A. Rogers was born in 1967, in Rolla, MO, and raised in Houston, TX. He received the B.A. and B.S. degrees in chemistry and physics from the University of Texas, Austin, in 1989, and the S.M. degrees in both physics and in chemistry in 1992, and the Ph.D. degree in physical chemistry in 1995 from the Massachusetts Institute of Technology, Cambridge, MA.

From 1995 to 1997, he was a Junior Fellow in the Harvard University Society of Fellows. He is now a Member of Technical Staff in Condensed Matter Physics at Bell Laboratories, Lucent Technologies, Murray Hill, NJ. His interests include techniques for micro and nanofabrication, ultrafast lasers for coherent time-resolved spectroscopy and metrology, high frequency acoustics, microelectromechanical systems, plastic electronics and active in-fiber grating devices.

Paulina Kuo received the B.S. degrees in both physics and materials science from the Massachusetts Institute of Technology, Cambridge, MA, in June 2000. She will be working towards the Ph.D. degree at Stanford University, Stanford, CA, in the Department of Applied Physics.

She has broad interests in optics and optical devices.

T. N. Nielsen, photograph and biography not available at the time of publication.

B. Mikkelsen, photograph and biography not available at the time of publication.